Additive Manufacturing Letters 5 (2023) 100122

Contents lists available at ScienceDirect

Additive Manufacturing Letters

journal homepage: www.elsevier.com/locate/addlet

Developing a best practice for sample preparation of additive manufactured AlSi10Mg for electron backscatter diffraction analysis

Erfan Maleki [a], Sara Bagherifard [a,*], Ludovica Rovatti [b], Rasheed Michael Ishola [b], Manoj Revuru [a], Mario Guagliano [a]

[a] Department of Mechanical Engineering, Politecnico di Milano, Milano, Italy
[b] Materials Analysis Laboratory, Politecnico di Milano, Milano, Italy

ARTICLE INFO

Keywords:
Additive manufacturing
AlSi10Mg, electron backscatter diffraction (EBSD)
Microstructural characterization
Qualification

ABSTRACT

Microstructural characterization has a key role in analyzing the properties of additive manufactured materials. Electron backscatter diffraction (EBSD) can offer a unique set of information on the microstructural state of these materials. However, EBSD analyses is extremely sensitive to the quality of the prepared sample and requires a seamless preparation eliminating any risk of contamination, oxidation or surface imperfections. Despite the wide use of EBSD analysis in AM, there is no universally accepted sample preparation protocol and the variety and sequence of the steps that can guarantee high quality data remain unclear. In this study, the efficiency of sample preparation methods with various final steps of vibrational polishing, vibrational polishing + cleaning, vibrational polishing + electro-chemical polishing and vibrational polishing + chemical etching was surveyed and compared for EBSD analyses of notched AM AlSi10Mg part. The obtained results help selecting the most efficient approach indicating that vibrational polishing + chemical etching with hit rate of 95.41% lead to the lowest zero solutions followed by vibrational polishing + electro-chemical polishing, vibrational polishing + pad cleaning and just vibrational polishing, respectively.

1. Introduction

Additive manufacturing (AM) technologies are getting notable attention thanks to their efficiency and flexibility in fabrication of complex components particularly in aerospace, automotive and medical applications [1–3]. With the advancement of AM technologies in various sectors, there is also an urgent need to develop roadmaps and guidelines for characterization of AM material, their qualification and certification [4–6]. There has been a collective effort towards developing qualification and characterization standards to address the required procedures and enhance the knowledge on material properties in the AM field; however, many aspects of these materials are still not adequately analyzed including surface quality, and microstructure [7–9]. The microstructure of AM materials, significantly affected by fusion and solidification processes, is one of the key factors for specifying their structure–property relationship [10–13]. Microstructural features such as distributions of grain shape and size, crystallographic texture, solidification structures and compositional variations considerably affect the mechanical properties [14]. Therefore, high accuracy microstructural characterizations can play a critical role in understanding, predicting and modulating the performance of AM materials. Based on the scale of microstructural features in AM materials ranging from grain length (< 0.2 mm), cell diameter (< 1 μm) to cell wall thickness (< 150 nm) and impurities (< 1 nm), different approaches of electron backscatter diffraction (EBSD), scanning electron microscopy (SEM), transmission electron microscopy (TEM) and high-angle annular dark-field (HAADF) scanning can be used [15].

Among the mentioned microstructural characterization methods, besides covering a wide range of characterization scales via EBSD, this method has unique advantages such as high-resolution observation of grains and grain boundary types as well as phase transformations, mapping of phase/orientations and also direct statistical measurement and quantitative analyses [16]. In addition, by post-processing of EBSD results different factors such as dislocation densities, dynamic recrystallizations, stress concentrations and plastic strains can also be estimated [17,18]. For a successful EBSD analyses, careful sample preparation is essential. Perfect preparation of the samples is one of the most challenging steps significantly affecting the quality of EBSD signals generated within a small interaction volume located at the surface of a sample with a penetration depth typically less than 50–100 nm. There should be no contamination, oxidation, imperfection, or scratches, on the final prepared surface [19,20]. As EBSD pattern quality is extremely sensitive

* Corresponding author.
E-mail address: sara.bagherifard@polimi.it (S. Bagherifard).

https://doi.org/10.1016/j.addlet.2023.100122
Received 18 November 2022; Received in revised form 11 January 2023; Accepted 20 January 2023

Table 1
Different sample preparation methods for EBSD analyses of AM materials.

Material	AM technology	Preparation method	Reference
AlSi10Mg	Laser powder bed fusion (LPBF)	Mechanical polishing followed by chemical-mechanical polishing using 0.05 μm colloidal silica suspension	[28]
Ti−6Al−4V	Plasma welding deposition (PWD)	Mechanical polishing followed by chemical-mechanical polishing using 0.4 μm colloidal alcohol-silica suspension	[29]
AlSi10Mg	LPBF	Mechanical polishing followed by chemical-mechanical polishing using 0.005 μm colloidal silica suspension	[30]
AlSi10Mg	LPBF	Mechanical polishing followed by chemical-mechanical polishing using 0.04 μm colloidal silica suspension	[31]
AlSi10Mg	LPBF	Mechanical and chemical-mechanical polishing followed by electro-chemical polishing using 10% perchloric acid and 90% methanol with voltage of 30 V and time of 2 s	[32]
Graded steel	Direct laser metal deposition (DLMD)	Mechanical and chemical-mechanical polishing followed by electro-chemical polishing using 10% perchloric acid and 90% methanol with voltage of 30 V and time of 20 s	[33]
AlF357 and AlSi10Mg	LPBF	Mechanical and chemical-mechanical polishing followed by vibrational polishing using 0.02 μm colloidal silica suspension	[34]
4130 low-alloy steel	LPBF	Mechanical polishing followed by chemical-mechanical polishing using 0.05 μm colloidal silica suspension	[35]
AlSi10Mg	LPBF	Mechanical polishing followed by chemical-mechanical polishing using 0.04 μm colloidal silica suspension	[36]
AlSi10Mg	Direct metal laser sintering (DMLS)	Mechanical polishing followed by chemical-mechanical polishing using 0.05 μm colloidal silica suspension	[37]
AlSi10Mg	LPBF	Mechanical polishing followed by chemical-mechanical polishing using 0.05 μm colloidal silica suspension	[38]

to the integrity of the crystallographic lattice on the surface of the prepared sample, additional preparation steps with respect to the normal polishing steps should be carried out to remove the introduced crystal damages [21]. Aluminum alloys are known to be predominantly challenging to correctly prepare for EBSD analysis when compared to other materials such as steels. This is no limited to AM materials but in general even for conventionally fabricated Al alloys, the sample preparation for EBSD analysis is more [22]. On these soft materials, mechanical polishing can cause further complexity as it may introduce a thin distorted surface layer, obscuring the underlying real microstructure. The presence of secondary phases further complicates the preparation process, as each phase may respond in different manner to the preparation steps. Considering these challenges various approaches have been suggested for preparation of these alloys [23]. Although EBSD analyses have been widely used for microstructural characterization of AM materials [24–27], no standard methods are reported for preparation of the samples before this analysis and a wide variety of methods with varying sequences are reported for AM materials in the literature as summarized in Table 1.

It can be observed that mechanical polishing (MP) followed by chemical-mechanical polishing (CMP) using colloidal silica suspension were applied in all preparation methods. However, in some cases additional steps of electro-chemical polishing (ECP) or vibrational polishing (VP) were also considered as the final steps to further enhance the quality of surface preparation. All mentioned sample preparation methods for EBSD were used for observation of core microstructure. However, it is known that sample preparation for microstructural characterization of the surface layer is even more challenging.

In this study, we assess the efficiency of different sample preparation methods for EBSD analyses of surface layer in the case of LPBF AlSi10Mg samples were investigated. Four different EBSD sample preparation methods with final steps of vibrational polishing, vibrational polishing + cleaning, vibrational polishing + electro-chemical polishing and vibrational polishing + chemical etching were applied and their efficiency performance were compared in terms of indexed fraction using the hit rate parameter of EBSD analyses.

2. Experimental procedures

2.1. Material and AM notched part

Notched LPBF AlSi10Mg samples were built vertically by SLM 500 HL systems (SLM Solution Group AG, Germany) using gas atomized (employing Argon (AR) as inert gas in atomization process) spherical powder (SLM solutions Group AG, Germany) with mean diameter of 44.5 μm. Optimized LPBF process parameters including spot diameter of 78 μm, laser power of 350 W, scan speed of 1150 mm/s, layer thickness of 50 μm, hatch distance of 170 μm and scanning strategy of 67° rotation between subsequent layers as well as contour remelting were used. Fig. 1a presents the shape and size of the notched part with considered supports for the manufacturing process. After supports removal (SR) to modify the surface quality and decrease the surface roughness of the as-built (AB) sample, chemical surface post-treatment of ECP was applied using a bath of 400 mL solution with 94% Acetic acid (CH_3COOH) + 6% Perchloric (HClO4) acid with voltage of 15 V for 240 s. The porosity of the samples were analyzed via Nikon Eclipse LV150NL optical microscope (OM, Nikon Corporation, Tokyo, Japan). Surface morphology was assessed using Zeiss EVO50 SEM (Carl Zeiss Microscopy, Jena, Germany) and contactless approach using an InfiniteFocus confocal microscope (Alicona, Austria) was employed for roughness measurements. Rectangular areas of 0.7 × 1 mm^2 were considered on the cylindrical parts of the samples below the notched area, where nine acquisitions were collected per sample and merged together with 5% overlap. It should be noted that three different paths were considered for roughness measurement and the mean value was reported for each case. Fig. 1b depicts the longitudinal cross-section of the AB and AB + SR + ECP samples demonstrating sub-surface porosities around the notched area. It can be observed that most of the porosities are located near to the upper notch face and notch root. Average porosity of about 0.6% was obtained for both AB and AB + SR + ECP samples. Fig. 1c indicates the SEM surface morphologies of AB and AB + SR + ECP samples. In addition, the considered area for confocal observation in AB and AB + SR + ECP samples are shown in Fig. 1d. Surface roughness values (R_a values) of 8.37 and 3.31 μm were obtained for AB and AB + SR + ECP samples, respectively revealing the high efficiency of ECP for roughness reduction as a post-processing method.

2.2. Microstructural characterization

For microstructural characterization, firstly the cylindrical samples were cut in longitudinal cross-sections with respect to the build direction and then were mounted using PolyFast conductive resin (Struers, Denmark). Different polishing methods of MP, CMP and VP, were respectively used as base preparation methods. For MP, initially different manual grinding steps were performed using sandpapers from P180 to P2500 each for 3 min with a rotational speed of 180 rpm using wa-

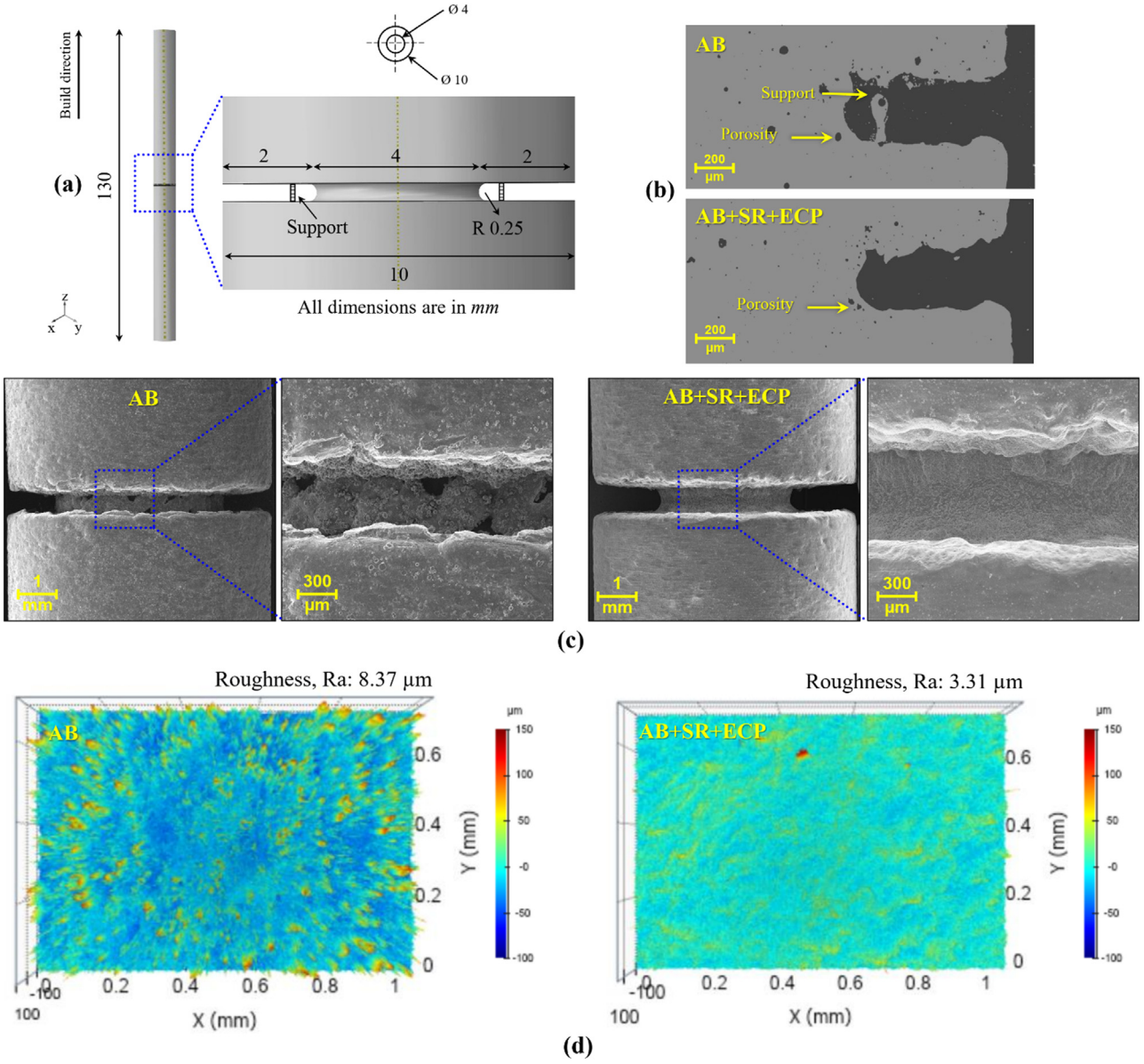

Fig. 1. (a) Shape and size of the notched part with considered supports for manufacturing (b) longitudinal cross-section of the AB and AB + SR + ECP samples demonstrating sub-surface porosities around the notched area (c) surface morphologies and the corresponding surface roughness (Ra values) of AB and AB + SR + ECP samples.

ter lubricant in a Mod MP311T polishing device (Hitech Europe, Italy). Then the samples were further polished using an automatic polishing equipment of Tegramin-25 (Struers, Denmark) with 2 water based polycrystalline diamond suspensions sequentially with abrasive size of 3 and 1 μm. The parameters were set to 10 N force, 150 rpm rotational speed (with counter-rotations between sample and the pad) and 240 s polishing time. Afterwards, CMP was carried out using 0.05 µm colloidal silica suspension by automatic polishing with parameters of 5 N force, 50 rpm rotational speed (with counter-rotations between sample and the pad), 300 s polishing. After MP and CMP, VP as a final step of base preparation method was performed using ATM SAPHIR VIBRO device (ATM Advanced Materialography, Germany). CMP was performed using 150 ml of 0.05 µm colloidal silica suspension with pad vibration frequency of 90 Hz and 190 g additional weight for the duration of 90 min.

As additional steps to the basic preparation method, 3 different processes of cleaning, ECP and chemical etching (CE) were considered here. In the case of cleaning, the surface of vibro-polished sample was cleaned by distilled water and soft pad with rotational speed of 40 rpm for 2 min. In the case of ECP, the vibro-polished surface was electro-chemically polished with a solution of acetic acid (94%) and perchloric acid (6%) at a voltage of 40 V for 4 s. In addition, in the last considered process of CE, vibro-polished surface was chemically etched for 4 s in Keller's reagent (95% pure H2O, 1% HF, 1.5% HCl, 2.5% HNO3). It should be mentioned that after finishing the additional steps, the surfaces of the samples were immediately covered by distilled water and dried by heated air and then kept in a vacuum chamber.

After preparation of the samples, microstructural characterization was performed using a high-resolution Zeiss Sigma 500 VP field-emission scanning electron microscope (FE-SEM, Carl Zeiss Microscopy GmbH, Jena, Germany) equipped with EBSD and energy dispersive spectrometry (EDS) (Oxford instruments, High Wycombe, United Kingdom). The associated AZtecHKL software was used to post-process the data. EBSD analyses were carried out by an accelerating voltage of 20 KV,

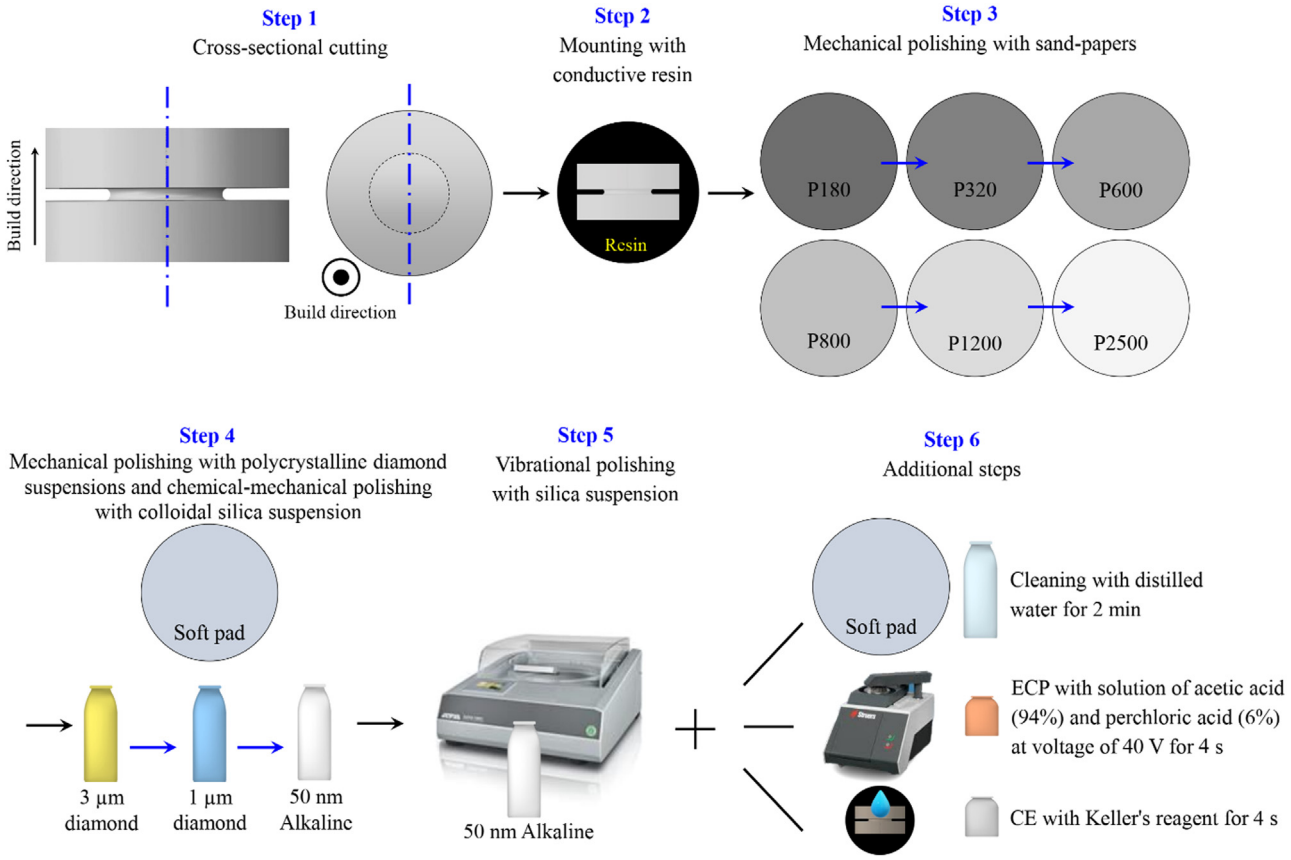

Fig. 2. Steps of the considered methods for sample preparation for EBSD analysis of LPBF AlSi10Mg.

70° sample tilt, 1 µm step size, 10 detected bands, camera binning mode speed of 311 × 256 pixels and the camera exposure time of 40.96 ms. The steps of the considered sample preparation methods for EBSD analysis of LPBF AlSi10Mg are schematically presented in Fig. 2. It should be noted that accurate phase fraction analysis has a key role in EBSD microstructural characterization of alloys as it can be essential to also quantify the effects of heat treatment or mechanical deformation on inducing heterogeneity. Particularly in AM materials, due to the intrinsic nonequilibrium solidification, which causes additional challenges for the proper quantification of phase fraction, considering the influence of samples preparation with different methods should be considered [39]. In this study, to avoid the effects of material heterogeneity and to get higher resolution, Si phase was not considered for diffraction due to its very small quantity in the Al matrix and thus only the crystallographic parameters of Al phase were taken into account. Also, all methods were applied o the same sample.

3. Results and discussions

Microstructural characterizations with focus on surface layer features in the notch root area of AB + SR + ECP sample were carried out considering different sample preparation methods. SEM micrographs and EBSD results in terms of band contrast, Al phase map and inverse pole figures (IPF-Z) were obtained for prepared samples with final steps of VP, VP + Cleaning, VP + ECP and VP + CE as shown in Fig. 3. All the applied methods for sample preparation were applied on one particular sample for better comparison. As observed in Fig. 1b, most of the porosities were located around notched area of the AB + SR + ECP sample; thus, this area was chosen for microstructural characterizations as a worst-case scenario. Considering SEM micrographs, all the prepared samples were finely polished without any scratches. However, some contaminations and stains, indicated by yellow arrows, can be observed clearly in the SEM images of the samples prepared with VP, and VP + Cleaning. These contaminations can be clearly distinguished from the sub-surface porosities. On the other hand, in the case of samples prepared with VP + ECP and VP + CE, no clear contaminations could not be detected in the SEM micrographs.

Dealing with the results of EBSD analyses, band contrast images reveal the contaminations and surface quality more clearly. In the samples prepared with VP, VP + Cleaning and VP + ECP relatively large particles with size of about 20–50 µm were placed in some of the subsurface porosities. While in the sample prepared with VP + CE rather than porosities no pollution can be observed. Considering Al phase maps of the samples prepared with different methods, it can be observed that in the corresponding areas to contaminations and porosities, zero solutions were obtained. The reflection of achieved zero solutions for detecting the Al phase can be clearly seen in the IPF-Z maps, which indicate the grains orientations. The results indicate that the prepared sample with VP + CE had the lowest zero solutions fraction followed by the samples prepared with VP + ECP, VP + Cleaning and VP, respectively. The columnar growth of grains along build direction with the domination of (001) orientation can be seen in the IPF-Z maps of LPBF AlSi10Mg material. Fig. 4 depicts the histograms of the band contrast maps of the prepared samples with different methods demonstrating quantitative comparison of the considered methods. It can be clearly observed that prepared sample with VP + CE had the highest gray levels followed by the samples prepared with VP + ECP, VP + Cleaning and VP, respectively.

EDS analyses were also performed on the samples prepared with different methods to specify the source of the contaminations. For instance, the elemental EDS maps of sample prepared with VP + Cleaning is presented in Fig. 5. The results indicate that silica (silicon dioxide)-

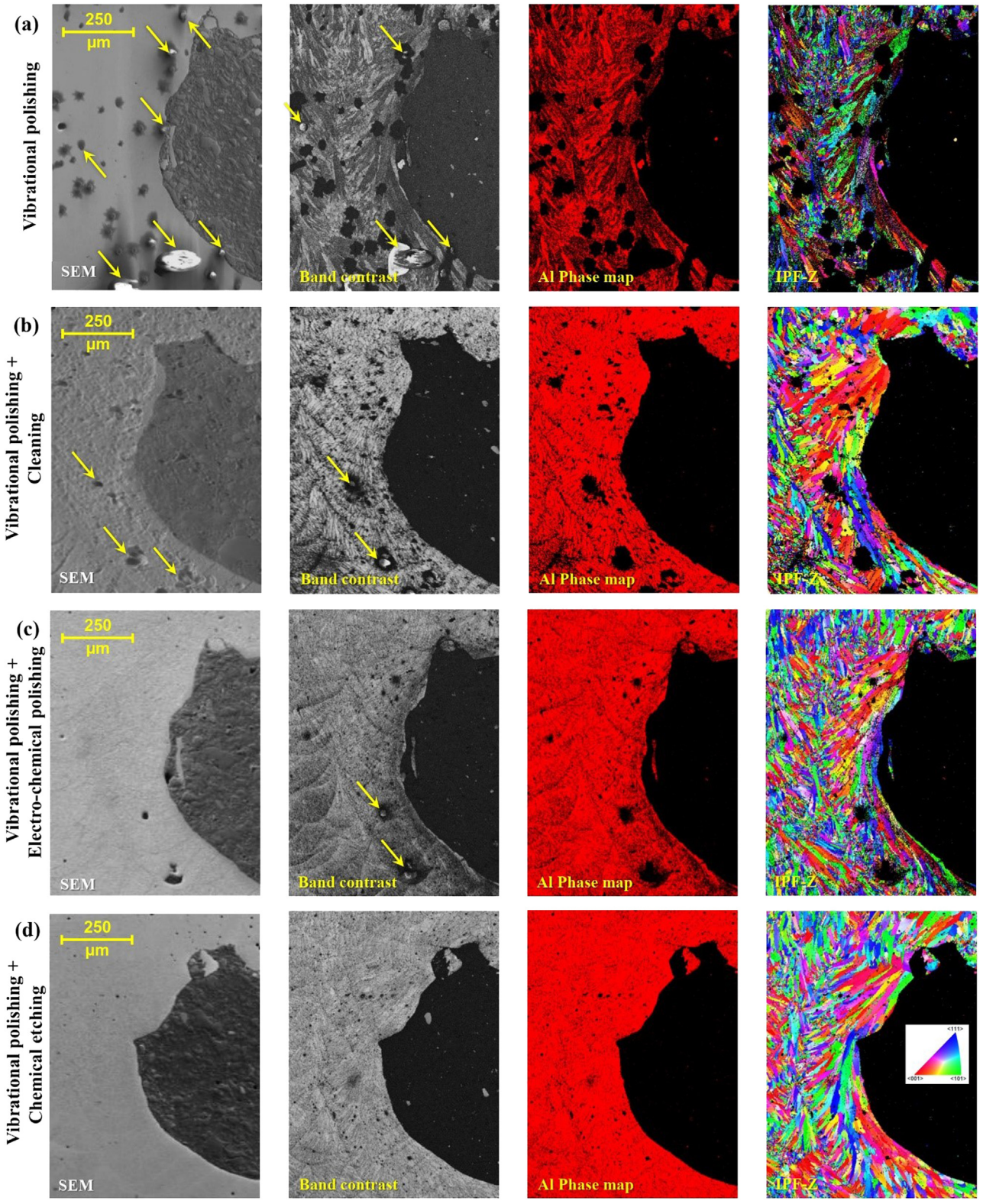

Fig. 3. SEM micrographs and EBSD results in terms of band contrast, Al phase and IPF-Z maps obtained for samples prepared with final steps of (a) VP, (b) VP + Cleaning, (c) VP + ECP and (d) VP + CE.

rich particles, mostly located inside the pores, can be specified as the main source of contamination. This point can be seen clearly in the corresponding EDS maps of Si and O demonstrating higher fraction of wt% (brighter phase) in the mentioned areas. Comparison of the sample preparation methods reveal that, additional steps of CE, ECP and Cleaning had respectively the highest effects on removal of the residual silica particles for vibro-polished surface.

The sharpness of the obtained diffraction pattern from EBSD analysis can be considered as one of the factors for analyzing the final image quality [40,41]. Fig. 6a schematically reveals the positions of the two

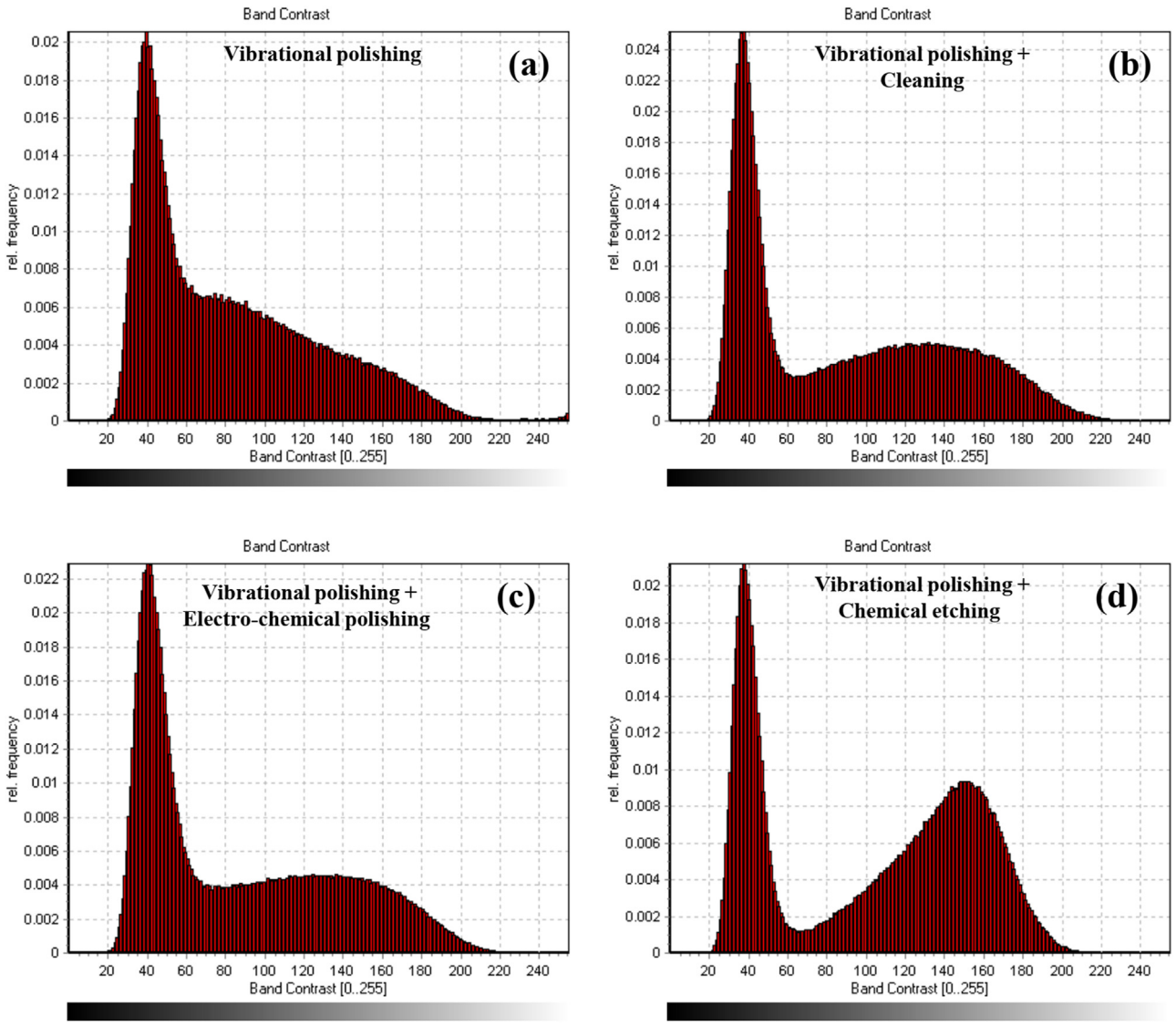

Fig. 4. Histograms of the band contrast maps for the prepared samples with (a) VP, (b) VP + Cleaning, (c) VP + ECP and (d) VP + CE.

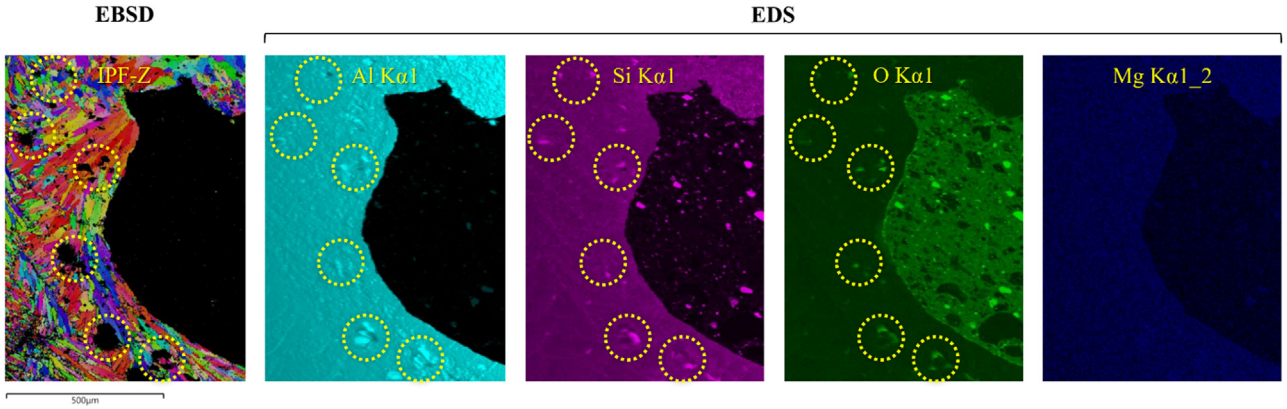

Fig. 5. EDS maps of sample prepared with VP + Cleaning in terms of Al, Si, O and Mg elements.

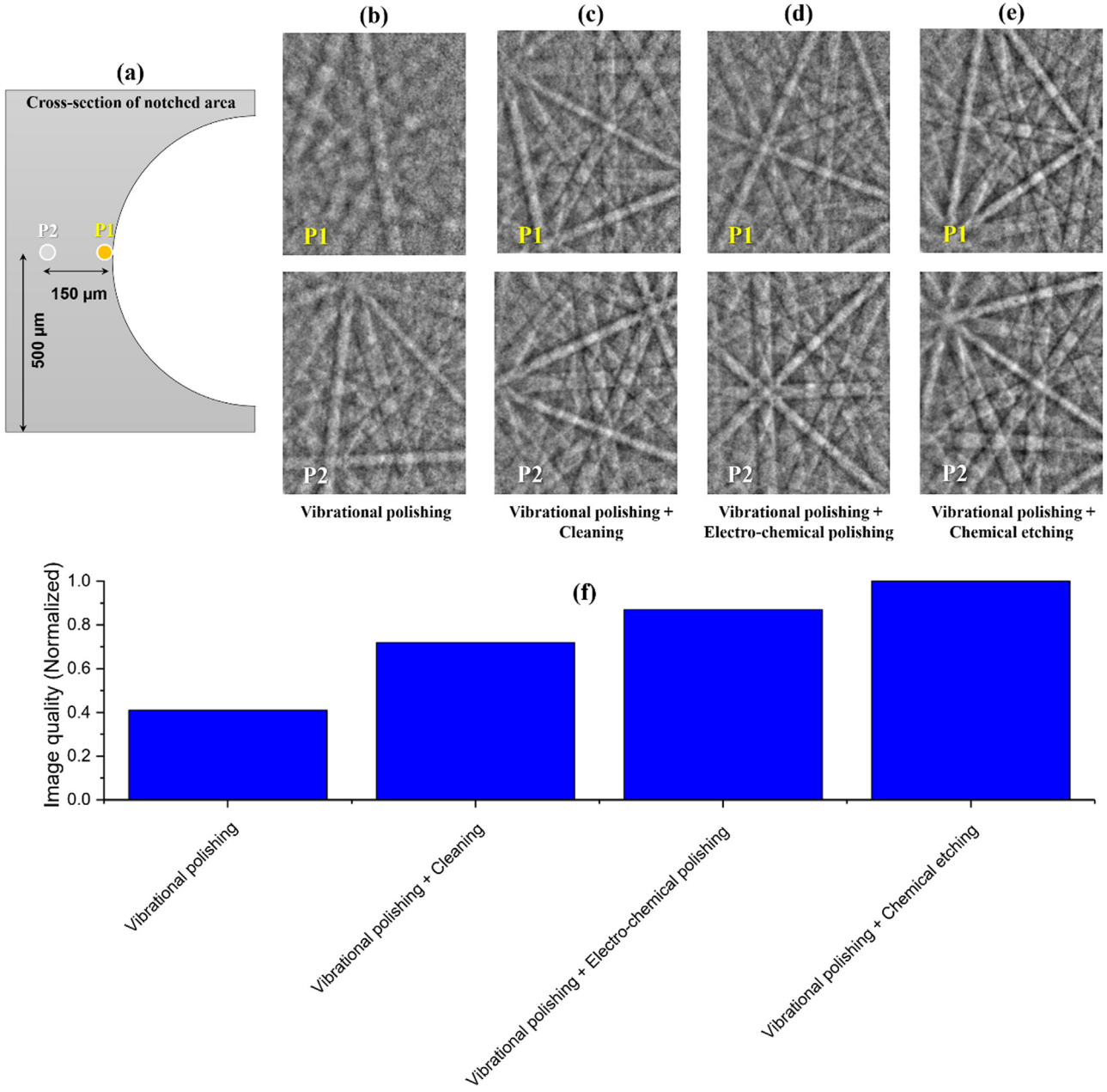

Fig. 6. (a) Schematical illustration of the positions of the two considered points of P1 and.

considered points for getting the diffraction patterns for all sets of samples. One point was considered very close to the notch root (P1) and the other one was located with 150 µm spacing on the notch root direction (P2). The corresponding patterns in points P1 and P2 for the samples prepared with different methods of VP, VP + Cleaning, VP + ECP and VP + CE are presented in Fig. 6b to 6e, respectively. It can be observed that by applying additional steps after VP the quality of diffraction patterns were improved and the sharpness of the bands increased; the sample prepared with VP + CE had the highest pattern contrast followed by the samples prepared with VP + ECP, VP + Cleaning and VP, respectively. It should be mentioned that the presented patterns are not filtered. Pattern quality (PQ), which indicates the level of diffraction pattern sharpness, can be used as an index of EBSD image quality. PQ can be calculated by measurements of the contrast of the brighter bands in the pattern above background, for every analyzed pattern. Since the calculations are independent of EBSD indexing, the data are generated from all points on the analyzed sample surface, regardless of indexability or the state of the material beneath [42,43]. Fig. 6f depicts the normalized calculated image quality of all sets of samples by using PQ measurement. The results indicated that the sample prepared with VP + CE had the highest image quality followed by the samples prepared with VP + ECP, VP + Cleaning and VP, respectively.

P2 for getting the diffraction patterns for all sets of samples. The corresponding diffraction patterns in points P1 and P2 for the samples prepared with different methods of (b) VP, (c) VP + Cleaning, (d) VP + ECP and (e) VP + CE. (f) The normalized calculated image quality of all sets of samples by considering PQ measurement.

Hit rate obtained from EBSD analyses can be used as an index for specifying the quality of pattern observation. In this study, the obtained values of hit rate for each EBSD analyses of samples prepared with different methods were used for efficiency comparison. Fig. 7a depicts the obtained Euler orientation maps of the prepared samples with different methods. As we focused on the notch root of the LPBF AlSi10Mg sample, a considerable fraction of analyzed area was covered by resin. Therefore,

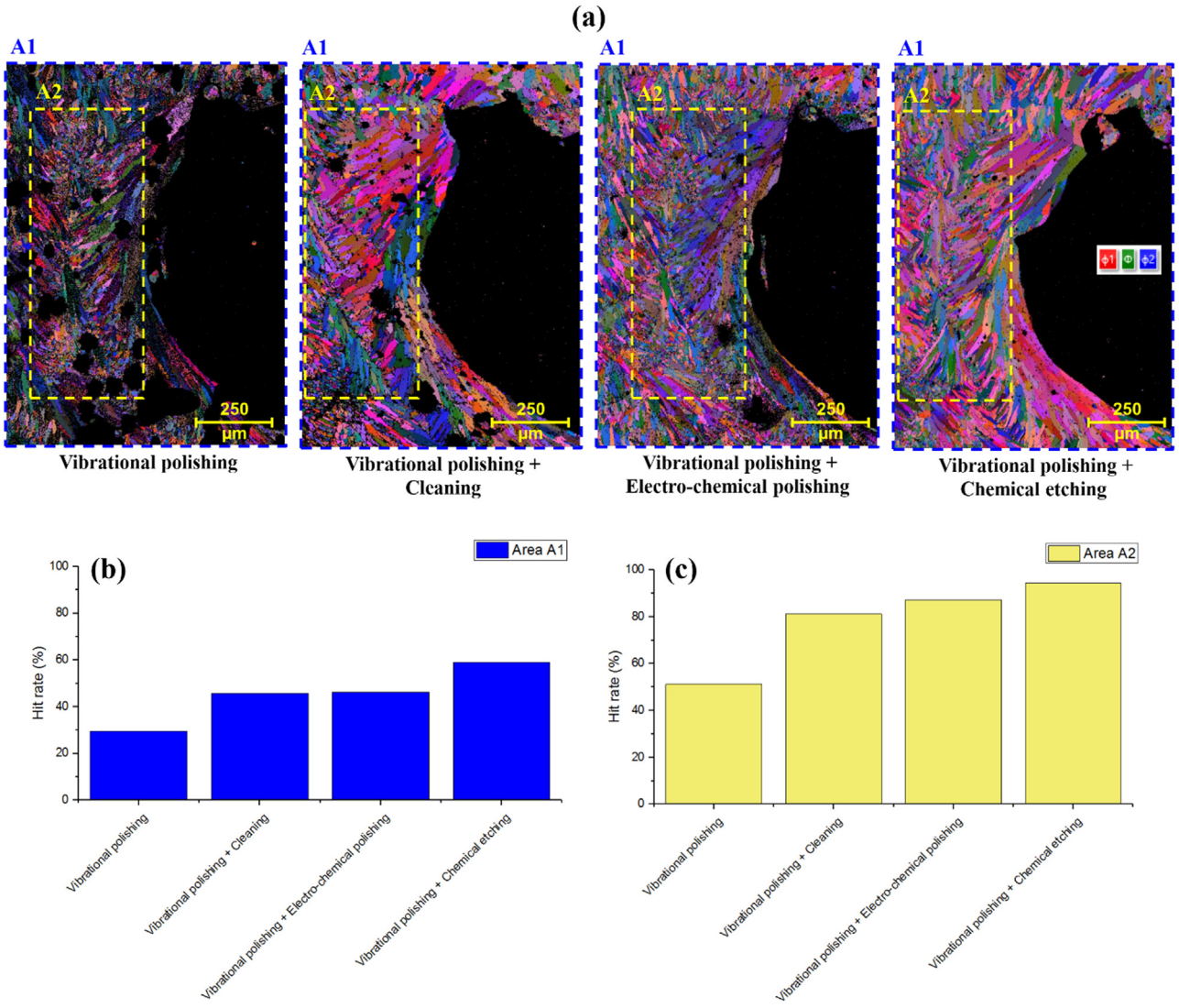

Fig. 7. (a) Obtained Euler orientation maps on samples prepared with different final steps of VP, VP + Cleaning, VP + ECP and VP + CE. The obtained values of hit rate considering different areas of (b) A1 and (c) A2 showing the highest acquired data for prepared sample with VP + CE.

the values of hit rate were obtained in two different areas. The whole scanned area for each EBSD analyses was considered as area A1 and a rectangular area located exactly beneath the notch root (without any mounting resin) was considered as area A2 to compensate for discrepancies in the hit rate due to possible presence of resin in the scanned area. As illustrated in Fig. 7b and 7c, the obtained values of hit rate reveal that sample prepared with VP + CE had the highest acquired data followed by samples prepared with VP + ECP, VP + Cleaning and VP methods, respectively. For example, considering area A2, 51.26, 81.12, 87.23 and 95.41% hit rates were obtained for sample prepared with methods of VP, VP + Cleaning, VP + ECP and VP + CE, respectively. We would like to highlight that the choice of the best practice shall be also adopted to the specific case study, since it is known that chemical and electrochemical etching are also sensitive to the state of plastic deformation in the material and thus can lead to inhomogeneous material removal in case of deformation inhomogeneity in different zones [42,44]; thus the final step should be selected also keeping this aspect into account.

For preparing EBSD samples properly it is important to understand that surface finish is not the only aspect to be focused on. It is also quite crucial that the layer of material sampled by EBSD is distortion free. Available data in the literature clearly reveal that there can be considerable deformation imparted into the sub-surface of a material during sample preparation [45,46]. In order to survey the effects of each sample prepartion method on inducing deformation to the surface layer, Kernel average misorientation (KAM) maps were obtained as presented in Fig. 8a. It can be observed that the average KAM values are significaltly reduced to about 0.55–0.6° after applying additional steps to VP comapred to the sole prepartion method of VP with mean KAM of 1.78° The obatained KAM results reflect the efficieny of the applied additional steps of Cleaning, ECP and CE for sample prepration of AM Al alloy for EBSD observations. The corresponding detailed KAM histograms of each sample prepation methods are depicted in Fig. 8b to 8e.

4. Conclusions

Herein, the efficiency of different sample preparation methods including vibrational polishing, vibrational polishing + cleaning, vibrational polishing + electro-chemical polishing and vibrational polishing + chemical etching for EBSD analyses of LPBF AlSi10Mg were investigated. The obtained results for various sample preparation methods revealed the silica-rich particles, mostly located inside the sub-surface porosities, as the main source of contamination. Comparison of different sample preparation methods indicated that the additional last step of chemical etching performed on vibro-polished surface, had the high-

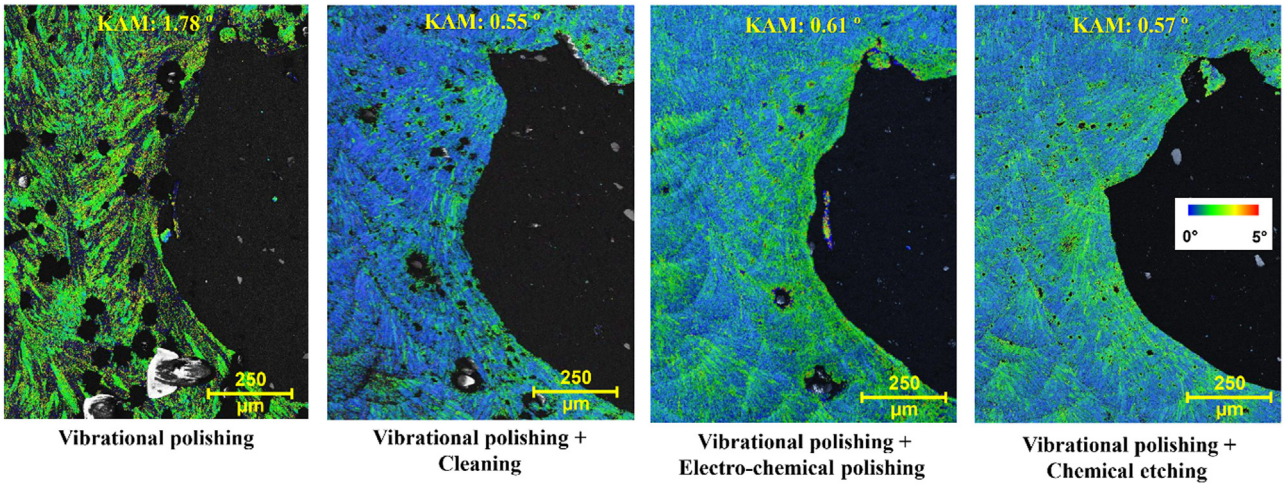

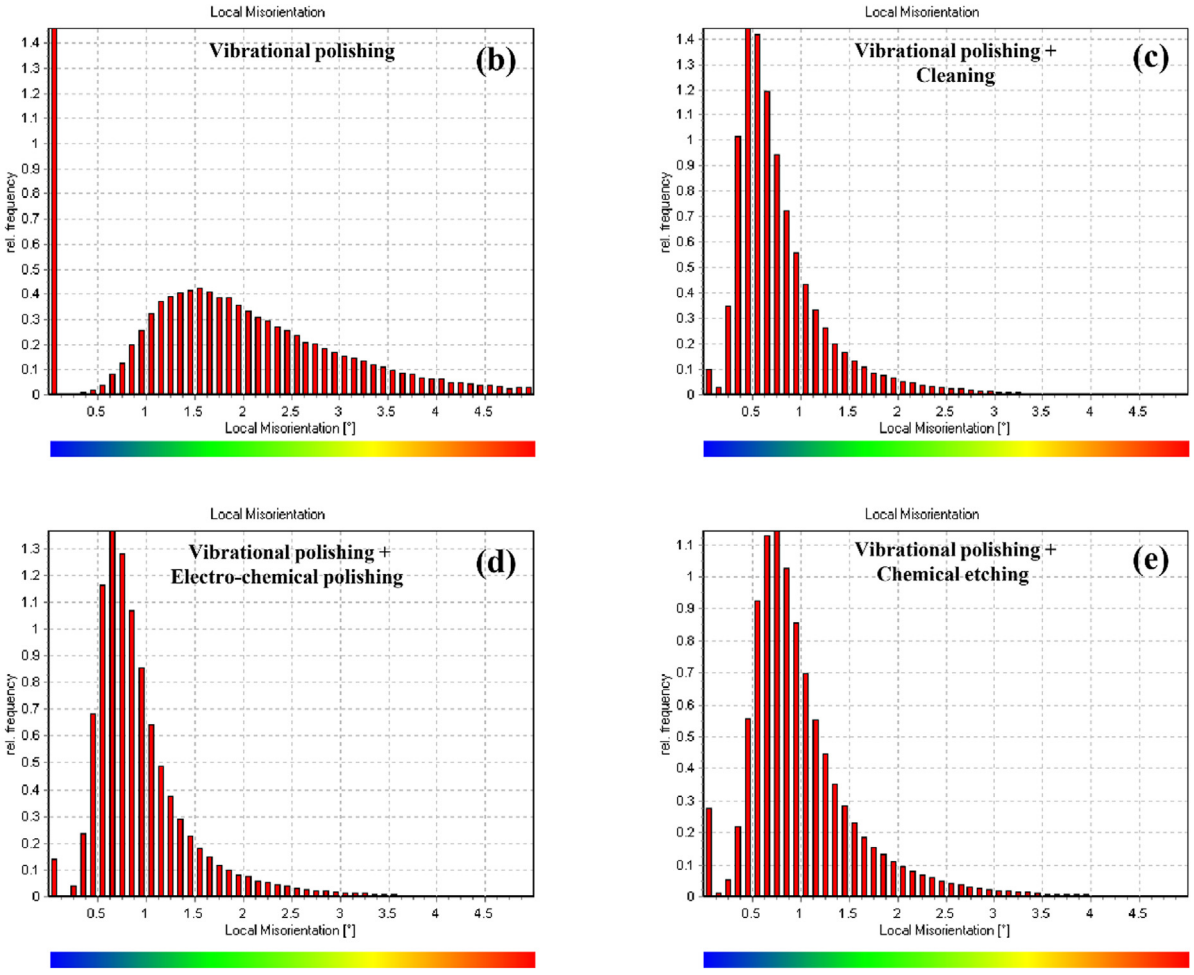

Fig. 8. (a) Obtained KAM maps for samples prepared with different final steps of VP, VP + Cleaning, VP + ECP and VP + CE. Detailed histogram of KAM values for samples prepared with (b) VP, (c) VP + Cleaning, (d) VP + ECP and (e) VP + CE.

est efficiency on the removal of the residual silica particles and thus led to the highest surface quality, without inducing any surface stresses and defects. The obtained hit rate values confirmed that sample prepared by vibrational polishing + chemical etching with 95.41% had the lowest zero solutions followed by vibrational polishing + electro-chemical polishing, vibrational polishing + Cleaning and vibrational polishing with hit rates of 87.23, 81.12 and 51.26%, respectively. Overall, chemical etching, as the last preparation step, led to better indexing and high-quality EBSD results, followed by electro-chemical polishing and Cleaning steps. Thus, it is recommended as the last step of surface preparation for EBSD analysis to guarantee high quality of results and facilitate accurate microstructural assessment of AM materials.

Declaration of Competing Interest

The authors declare that they have no known competing financial interests or personal relationships that could have appeared to influence the work reported in this paper.

Data availability

No data was used for the research described in the article.

References

[1] J.J. Lewandowski, M. Seifi, Metal additive manufacturing: a review of mechanical properties, Annu. Rev. Mater. Res. 46 (2016) 151–186, doi:10.1146/annurev–matsci-070115-032024.

[2] A. Yadollahi, N. Shamsaei, Additive manufacturing of fatigue resistant materials: challenges and opportunities, Int. J. Fatigue. 98 (2017) 14–31, doi:10.1016/j.ijfatigue.2017.01.001.

[3] E. Maleki, S. Bagherifard, M. Bandini, M. Guagliano, Surface post-treatments for metal additive manufacturing: progress, challenges, and opportunities, Addit. Manuf. 37 (2021) 101619, doi:10.1016/j.addma.2020.101619.

[4] D.L. Bourell, M.C. Leu, D.W. Rosen, Roadmap For Additive Manufacturing: Identifying the Future of Freeform Processing, Univ. Texas Austin, 2009.

[5] K. Jurrens, Energetics incorporated, measurement science roadmap for metal-based additive manufacturing, Addit. Manuf. (2013).

[6] J.M. Waller, B.H. Parker, K.L. Hodges, E.R. Burke, J.L. Walker, Nondestructive Evaluation of Additive Manufacturing State-of-the-Discipline Report, 2014.

[7] M. Seifi, A. Salem, J. Beuth, O. Harrysson, J.J. Lewandowski, Overview of materials qualification needs for metal additive manufacturing, JOM (2016), doi:10.1007/s11837-015-1810-0.

[8] T. DebRoy, H.L. Wei, J.S. Zuback, T. Mukherjee, J.W. Elmer, J.O. Milewski, A.M. Beese, A. Wilson-Heid, A. De, W. Zhang, Additive manufacturing of metallic components – Process, structure and properties, Prog. Mater. Sci. 92 (2018) 112–224, doi:10.1016/j.pmatsci.2017.10.001.

[9] M. Seifi, M. Gorelik, J. Waller, N. Hrabe, N. Shamsaei, S. Daniewicz, J.J. Lewandowski, Progress towards metal additive manufacturing standardization to support qualification and certification, JOM (2017), doi:10.1007/s11837-017-2265-2.

[10] Z. Liu, D. Zhao, P. Wang, M. Yan, C. Yang, Z. Chen, J. Lu, Z. Lu, Additive manufacturing of metals: microstructure evolution and multistage control, J. Mater. Sci. Technol. (2022), doi:10.1016/j.jmst.2021.06.011.

[11] P. Bajaj, A. Hariharan, A. Kini, P. Kürnsteiner, D. Raabe, E.A. Jägle, Steels in additive manufacturing: a review of their microstructure and properties, Mater. Sci. Eng. A. (2020), doi:10.1016/j.msea.2019.138633.

[12] E. Maleki, S. Bagherifard, O. Unal, M. Bandini, M. Guagliano, The effects of microstructural and chemical surface gradients on fatigue performance of laser powder bed fusion AlSi10Mg, Mater. Sci. Eng. A. 840 (2022) 142962, doi:10.1016/j.msea.2022.142962.

[13] E. Maleki, S. Bagherifard, O. Unal, M. Bandini, M. Guagliano, On the effects of laser shock peening on fatigue behavior of V-notched AlSi10Mg manufactured by laser powder bed fusion, Int. J. Fatigue 163 (2022) 107035, doi:10.1016/j.ijfatigue.2022.107035.

[14] T.M. Rodgers, H. Lim, J.A. Brown, Three-dimensional additively manufactured microstructures and their mechanical properties, JOM (2020), doi:10.1007/s11837-019-03808-x.

[15] Y.M. Wang, T. Voisin, J.T. McKeown, J. Ye, N.P. Calta, Z. Li, Z. Zeng, Y. Zhang, W. Chen, T.T. Roehling, R.T. Ott, M.K. Santala, P.J. Depond, M.J. Matthews, A.V. Hamza, T. Zhu, Additively manufactured hierarchical stainless steels with high strength and ductility, Nat. Mater. (2018), doi:10.1038/NMAT5021.

[16] E.V.D. Pereloma Elena, Phase transformations in steels 2 Diffusionless Transformations, High Strength Steels, Modelling and Advanced Analytical Techniques, 2012.

[17] E. Maleki, O. Unal, M. Bandini, M. Guagliano, S. Bagherifard, Individual and synergistic effects of thermal and mechanical surface post-treatments on wear and corrosion behavior of laser powder bed fusion AlSi10Mg, J. Mater. Process. Technol. 302 (2022) 117479, doi:10.1016/j.jmatprotec.2021.117479.

[18] E. Maleki, S. Bagherifard, F. Sabouri, M. Bandini, M. Guagliano, Hybrid thermal, mechanical and chemical surface post-treatments for improved fatigue behavior of laser powder bed fusion AlSi10Mg notched samples, Surf. Coatings Technol. 430 (2022), doi:10.1016/j.surfcoat.2021.127962.

[19] M.M. Nowell, R.A. Witt, B. True, EBSD sample preparation: techniques, tips, and tricks, Microsc. Microanal. (2005), doi:10.1017/s143192760550672x.

[20] P. Nowakowski, J. Schlenker, M. Ray, P. Fischione, Sample preparation using broad argon ion beam milling for electron backscatter diffraction (EBSD) analysis, Microsc. Microanal. (2016), doi:10.1017/s143192761600091x.

[21] S.I. Wright, M.M. Nowell, D.P. Field, A review of strain analysis using electron backscatter diffraction, Microsc. Microanal. (2011), doi:10.1017/S1431927611000055.

[22] Í. Carneiro, S. Simões, Recent advances in ebsd characterization of metals, Metals (Basel) (2020), doi:10.3390/met10081097.

[23] S. Singh, Y. Guo, B. Winiarski, T.L. Burnett, P.J. Withers, M. De Graef, High resolution low kV EBSD of heavily deformed and nanocrystalline Aluminium by dictionary-based indexing, Sci. Rep. (2018), doi:10.1038/s41598-018-29315-8.

[24] P. Yang, M.A. Rodriguez, L.A. Deibler, B.H. Jared, J. Griego, A. Kilgo, A. Allen, D.K. Stefan, Effect of thermal annealing on microstructure evolution and mechanical behavior of an additive manufactured AlSi10Mg part, J. Mater. Res. 33 (2018) 1701–1712, doi:10.1557/jmr.2018.82.

[25] J. Guan, Y. Jiang, X. Zhang, X. Chong, Microstructural evolution and EBSD analysis of AlSi10Mg alloy fabricated by selective laser remelting, Mater. Charact. 161 (2020) 110079, doi:10.1016/j.matchar.2019.110079.

[26] X. Wang, K. Chou, EBSD study of beam speed effects on Ti-6Al-4 V alloy by powder bed electron beam additive manufacturing, J. Alloys Compd. (2018), doi:10.1016/j.jallcom.2018.03.173.

[27] A. Hadadzadeh, B.S. Amirkhiz, J. Li, M. Mohammadi, Columnar to equiaxed transition during direct metal laser sintering of AlSi10Mg alloy: effect of building direction, Addit. Manuf. 23 (2018) 121–131, doi:10.1016/j.addma.2018.08.001.

[28] B. Amir, S. Samuha, O. Sadot, Influence of selective laser melting machine source on the dynamic properties of AlSi10Mg Alloy, Materials (Basel) 12 (2019), doi:10.3390/ma12071143.

[29] M. Borlaug Mathisen, L. Eriksen, Y. Yu, O. Jensrud, J. Hjelen, Characterization of microstructure and strain response in Ti-6Al-4 V plasma welding deposited material by combined EBSD and in-situ tensile test, Trans. Nonferrous Met. Soc. China (English Ed. 24 (2014) 3929–3943, doi:10.1016/S1003-6326(14)63553-6.

[30] A. Kempf, K. Hilgenberg, Influence of sub-cell structure on the mechanical properties of AlSi10Mg manufactured by laser powder bed fusion, Mater. Sci. Eng. A. (2020), doi:10.1016/j.msea.2020.138976.

[31] P. Li, Y. Kim, A.C. Bobel, L.G. Hector, A.K. Sachdev, S. Kumar, A.F. Bower, Microstructural origin of the anisotropic flow stress of laser powder bed fused AlSi10Mg, Acta Mater. 220 (2021), doi:10.1016/j.actamat.2021.117346.

[32] M. Liu, K. Wei, X. Zeng, High power laser powder bed fusion of AlSi10Mg alloy: effect of layer thickness on defect, microstructure and mechanical property, Mater. Sci. Eng. A. 842 (2022) 143107, doi:10.1016/j.msea.2022.143107.

[33] Q. Wang, S. Zhang, C.H. Zhang, C. Wu, J. Wang, J. Chen, Z. Sun, Microstructure evolution and EBSD analysis of a graded steel fabricated by laser additive manufacturing, Vacuum (2017), doi:10.1016/j.vacuum.2017.03.021.

[34] J.P. Isaac, S. Lee, S. Thompson, A. Saharan, N. Shamsaei, H.V. Tippur, Role of build orientation on quasi-static and dynamic fracture responses of additively manufactured AlF357 and AlSi10Mg alloys, Addit. Manuf. 59 (2022) 103080, doi:10.1016/j.addma.2022.103080.

[35] M. Abdelwahed, S. Bengtsson, M. Boniardi, A. Casaroli, R. Casati, M. Vedani, Materials Science & Engineering A An investigation on the plane-strain fracture toughness of a water atomized 4130 low-alloy steel processed by laser powder bed fusion, Mater. Sci. Eng. A. 855 (2022) 143941, doi:10.1016/j.msea.2022.143941.

[36] Q. Tan, J. Zhang, N. Mo, Z. Fan, Y. Yin, M. Bermingham, Y. Liu, H. Huang, M.X. Zhang, A novel method to 3D-print fine-grained AlSi10Mg alloy with isotropic properties via inoculation with LaB6 nanoparticles, Addit. Manuf. 32 (2020) 101034, doi:10.1016/j.addma.2019.101034.

[37] A. Hadadzadeh, B. Shalchi Amirkhiz, A. Odeshi, J. Li, M. Mohammadi, Role of hierarchical microstructure of additively manufactured AlSi10Mg on dynamic loading behavior, Addit. Manuf. 28 (2019) 1–13, doi:10.1016/j.addma.2019.04.012.

[38] E. Maleki, S. Bagherifard, S.M.J. Razavi, M. Riccio, M. Bandini, A. du Plessis, F. Berto, M. Guagliano, Fatigue behaviour of notched laser powder bed fusion AlSi10Mg after thermal and mechanical surface post-processing, Mater. Sci. Eng. A. 829 (2022) 142145, doi:10.1016/j.msea.2021.142145.

[39] F. Zhang, M.R. Stoudt, S. Hammadi, C.E. Campbell, E.A. Lass, M.E. Williams, How austenitic is a martensitic steel produced by laser powder bed fusion? A cautionary tale, Metals (Basel) (2021), doi:10.3390/met11121924.

[40] S.I. Wright, M.M. Nowell, EBSD image quality mapping, Microsc. Microanal. (2006), doi:10.1017/S1431927606060090.

[41] R. Hielscher, F. Bartel, T.B. Britton, Gazing at crystal balls: electron backscatter diffraction pattern analysis and cross correlation on the sphere, Ultramicroscopy (2019), doi:10.1016/j.ultramic.2019.112836.

[42] S. Sitzman, G. Nolze, M. Nowell, EBSD pattern quality and its use in evaluating sample surface condition, Microsc. Microanal. (2010), doi:10.1017/s143192761005467x.

[43] G. Sparks, P.A. Shade, M.D. Uchic, S.R. Niezgoda, M.J. Mills, M. Obstalecki, High-precision orientation mapping from spherical harmonic transform indexing of electron backscatter diffraction patterns, Ultramicroscopy (2021), doi:10.1016/j.ultramic.2020.113187.

[44] C. Fressengeas, B. Beausir, C. Kerisit, A.L. Helbert, T. Baudin, F. Brisset, M.H. Mathon, R. Besnard, N. Bozzolo, On the evaluation of dislocation densities in pure tantalum from EBSD orientation data, Mater. Tech. (2018), doi:10.1051/mattech/2018058.

[45] D. Katrakova, F. Mücklich, Specimen preparation for electron backscatter diffraction - Part I: metals, Prakt. Metallogr. Metallogr. (2001).

[46] J.W. Signorelli, A. Roatta, N. De Vincentis, C. Schwindt, M. Avalos, R.E. Bolmaro, N. Bozzolo, Electron backscatter diffraction study of orientation gradients at the grain boundaries of a polycrystalline steel sheet deformed along different loading paths, J. Appl. Crystallogr. (2017), doi:10.1107/S1600576717009372.